Design and Test of a MEMS-Based High G Smart Sensor

Y. P. Wang, R. Q. Hsu, and C. W. Wu

***Abstract*—Most conventional G sensors use cantilever beams or axial springs as triggering devices. The reaction time of these conventional G sensors are often far too long. In many high G ($>$ 300 G) applications, they completely fail to function. This study proposed a microelectromechanical systems-based high G smart sensor, which not only functions at a very high G impact but also identifies the material when a projectile makes an impact on a hard object. This high G smart sensor is intended for use at 3000–21 000 G. The sensor was made of silicon and the triggering mechanism involves a cantilever and a spring structure. The mechanical sensitivity of the sensors can be adjusted to preset the triggering G value. Four sensors, each designated to trigger its own G value were integrated in a unit. Experiments demonstrated that this unit can identify the characteristics of an object.**

***Index Terms*—High G, microelectromechanical systems (MEMS), proof mass, smart sensor, spring.**

I. Introduction

MOST conventional G sensors use a cantilever beam or an axial spring in their triggering mechanisms as described by Wang [1].

For high G (>300 G) applications, the reaction time of conventional mechanical type G sensors is too long. Sometimes, the G sensor structures disintegrate (>5000 G).

Trimmer [2] proposed a unique model that demonstrated reducing the scale of a structure will decrease the time required for displacing a fixed point. Therefore, a smaller G sensor has a faster response. Some researchers [3] have designed shock sensors that have shorter reaction time than conventional sensors and mechanisms that are sufficiently robust against such impacts as occur when vehicles collide with hard objects. Min and Min [4] developed a device that can identify an object in real-time, but its processor required an enormous database to execute complex signal analysis. This investigation focuses mainly on using high G shock sensors to make a simple and cheap smart sensor with a real-time identification function that is effective when the sensor makes an impact on an object that consists of various materials.

The proposed microelectromechanical systems (MEMS)-based smart sensor is fabricated from silicon, whose Young's modulus [5] approaching 190 GPa, is close to that of steel (210 GPa). Moreover, silicon has virtually no mechanical hysteresis, and so is an ideal material for sensors and actuators.

Manuscript received March 20, 2010; revised July 12, 2010; accepted September 08, 2010. Date of publication September 27, 2010; date of current version February 11, 2011. The associate editor coordinating the review of this paper and approving it for publication was Dr. Patrick Ruther.

The authors are with the Department of Mechanical Engineering, National Chiao Tung University, Hsinchu 300, Taiwan (e-mail: anitawu.wlh@msa.hinet.net; rqhsu@mail.nctu.edu.tw; wuchihwe@mail.ntou.edu.tw).

Digital Object Identifier 10.1109/JSEN.2010.2079325

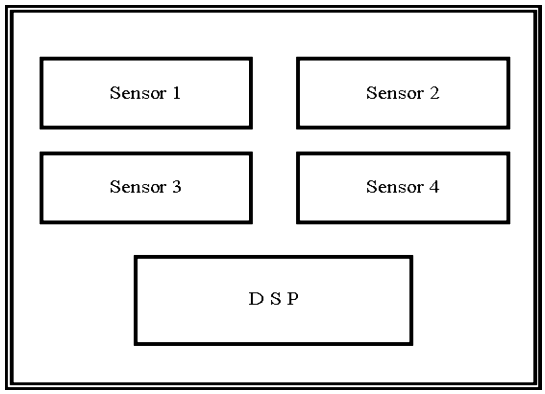

Fig. 1. Schematic of the smart sensor.

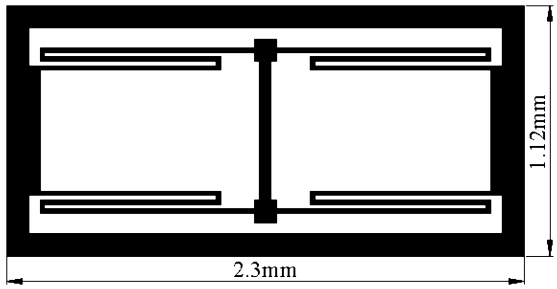

Fig. 2. Configuration of the micro G sensor.

II. Theoretical Analysis

Four types of G sensor were combined with a digital signal processor (DSP) to make a smart sensor with a real-time identification function. Fig. 1 schematically depicts the device. Fig. 2 presents in detail the dimensions of the proposed micro G sensor. The sensor has two main components—a spring, and a proof mass. The spring is divided into four sections and anchored on two sides of the sensor frame. The proof mass is located in the middle zone of the sensor and is linked to the four spring sections. This sensor uses a Mass-Damper-Spring Dynamic (MDS) System to trigger the cantilever mechanism.

Fig. 3 schematically depicts the MDS system. The dynamic equation of motion of the proof mass is given by 1-D lumped-system model that was proposed by Elwenspoek [6]

$$M\ddot{X}_{\text{out}} + D\dot{X}_{\text{out}} + KX_{\text{out}} = F = M\ddot{X}_{\text{in}} = Ma \quad (1)$$

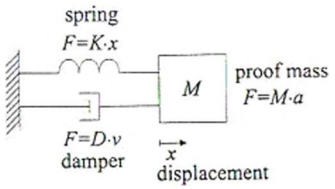

Fig. 3. Mass-spring-damping system.

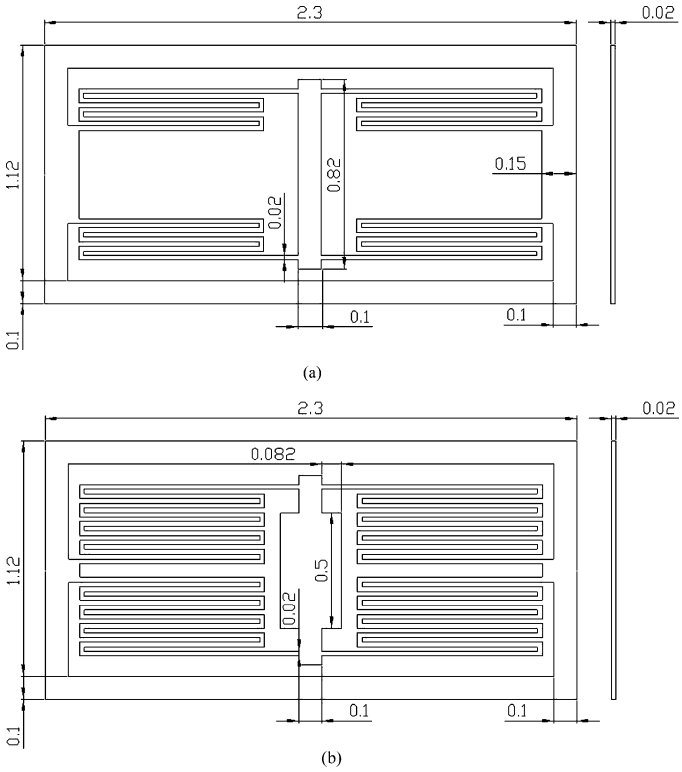

Fig. 4. Dimensions of two typical sensors (mm): (a) Type 2 and (b) Type 4.

where F represents the external force that acts on the frame, D is the damping factor, K is the effective spring constant of the elements, and M is the proof mass, which is attached to a fixed frame by one or more spring elements. The displacement $(\mathrm{x_{out}})$ is directly proportional to the acceleration $(\ddot{\mathrm{x}}_{\mathrm{in}})$ when the acceleration is constant. The (1) can be simplified to

$$X_{\mathrm{out}} = \left(\frac{M}{K}\right)\ddot{X}_{\mathrm{in}} = M_s\ddot{X}_{\mathrm{in}} \tag{2}$$

where $\mathrm{Ms} = (\mathrm{M/K})$ is the mechanical sensitivity of the system. Accordingly, the mechanical sensitivity of the system varies with the spring constant and the proof mass. The triggering G value of the sensor can be set by adjusting the mechanical sensitivity of the system.

III. Finite- Element Modeling

Four arrangements of spring and proof mass were designed. Table I shows detailed information concerning the design of the sensors. All proof masses have the same thickness of 20 μm; therefore, the ratio of these masses equals the ratio of their surface areas of the proof masses. Fig. 4 presents two of the sensor designs that are used in this investigation. The proof mass of type 2 is defined as having a mass of 1.0. Figs. 5 and 6 show one design of the shock sensor (type 4) that was manufactured using MEMS.

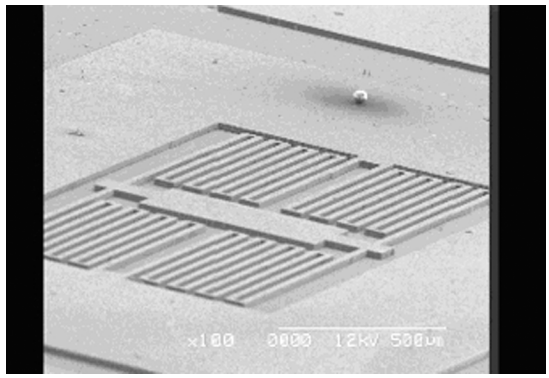

Fig. 5. SEM image of Type 4 sensor.

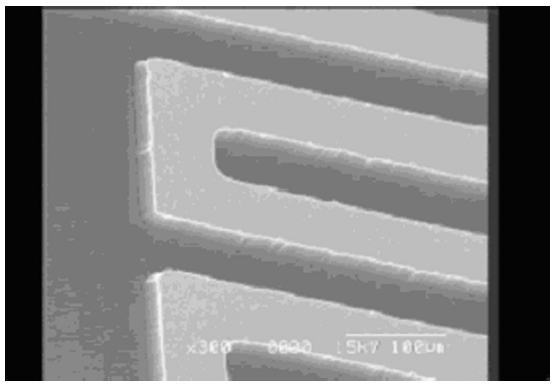

Fig. 6. SEM image of spring.

TABLE I
Detail Design Information

Type	Mass scale	Coil number	Kx (N/m)	Ky (N/m)	Kz (N/m)	Resonant frequency (kHz)
1	0.62	4	1058.1	32.3	28.6	19.0
2	1.00	8	721.3	22.2	19.7	11.9
3	1.00	12	508.3	15.4	13.7	8.8
4	2.24	16	410.6	12.2	10.8	6.2

Finite-element analyses were conducted using ANSYS version 8.0 and LS-DYNA [7] to determine the time-displacement relation of the proof mass when the sensor underwent an impact. The spring constant K was calculated by using ANSYS to simulate the proof mass displacement under various loads. Table I lists the spring constants of all of the sensors, showing $(\mathrm{K1} > \mathrm{K2} > \mathrm{K3} > \mathrm{K4})$.

In the simulation of the impact, a series of half-sine waves were applied to the sensors. The durations of the input half-sine waves were close to 100 μs in the range $\mathrm{G} = 10\,000$–$21\,000$, and close to 1 ms in the range $\mathrm{G} = 3000$–8000. Seven G values, ranging from 3000 to 21 000, were used in the simulation, consistent with (Mil-Std-810F).

IV. Simulation Results

In the dynamic simulations in the time domain, a shock wave (G-T curve) is applied to a G sensor, and the reaction time of

TABLE II
REACTION TIME (μS) OF THE MICRO-SENSORS

Sensor type	Reaction time (μs)						
	21000 G	20000 G	10000 G	8000 G	5000 G	4000 G	3000 G
Type 1	24.99	25.99	×	×	×	×	×
Type 2	21.99	22.99	33.99	40.99	×	×	×
Type 3	21.99	22.99	31.99	35.99	48.99	×	×
Type 4	21.99	22.99	31.99	35.99	44.99	50.99	65.99

Note × : The sensor does not trigger.

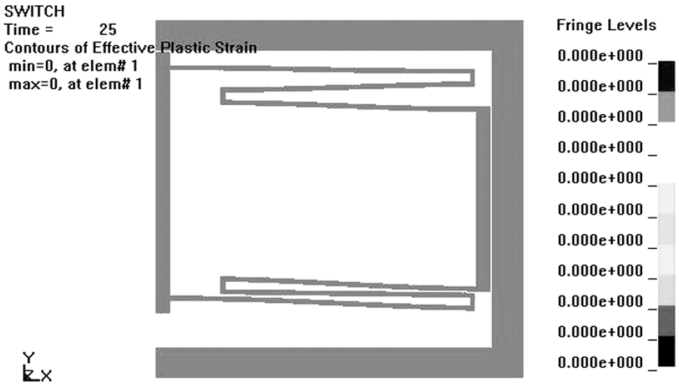

Fig. 7. Plastic strain of the type 1 sensor at 21 000 G.

the sensor is defined as the time for the proof mass to move from rest until it is in contact with the frame. (The displacement is 5.0E-03 cm.) When the proof mass comes into contact with the top frame, the built-in wiring triggers the sensor. If the proof mass does not reach the top frame, then the sensor is not triggered.

The assumptions made in the simulation were: a) the enclosure frame of the sensor is a rigid body; b) the sensor components are sufficiently large for principles of continuum mechanics to apply [8]; and c) the air damping effect can be neglected because the shock sensor is packaged in a vacuum environment. The projectile penetrates directly into the targets with no oblique angle. The simulation reveals that when the spring constant was reduced or the proof mass was increased, the triggering G value and the reaction time decreased (Table II).

According to Fig. 7, the simulation of the induced strain of the type 1 sensor, even at G = 21 000, indicated no observable plastic strains in the structural members. The simulation results in Fig. 8 indicate that the proof mass was displaced only in the y direction. No significant interference in the directions of the x and z axes was observed. Consequently, the stability of the sensor was very good.

The smart sensor that was developed herein incorporates four high G sensors, listed in Table II, and a DSP. The high G sensors were designed to trigger at different decelerations. When a projectile that carries this smart sensor penetrates a target, the

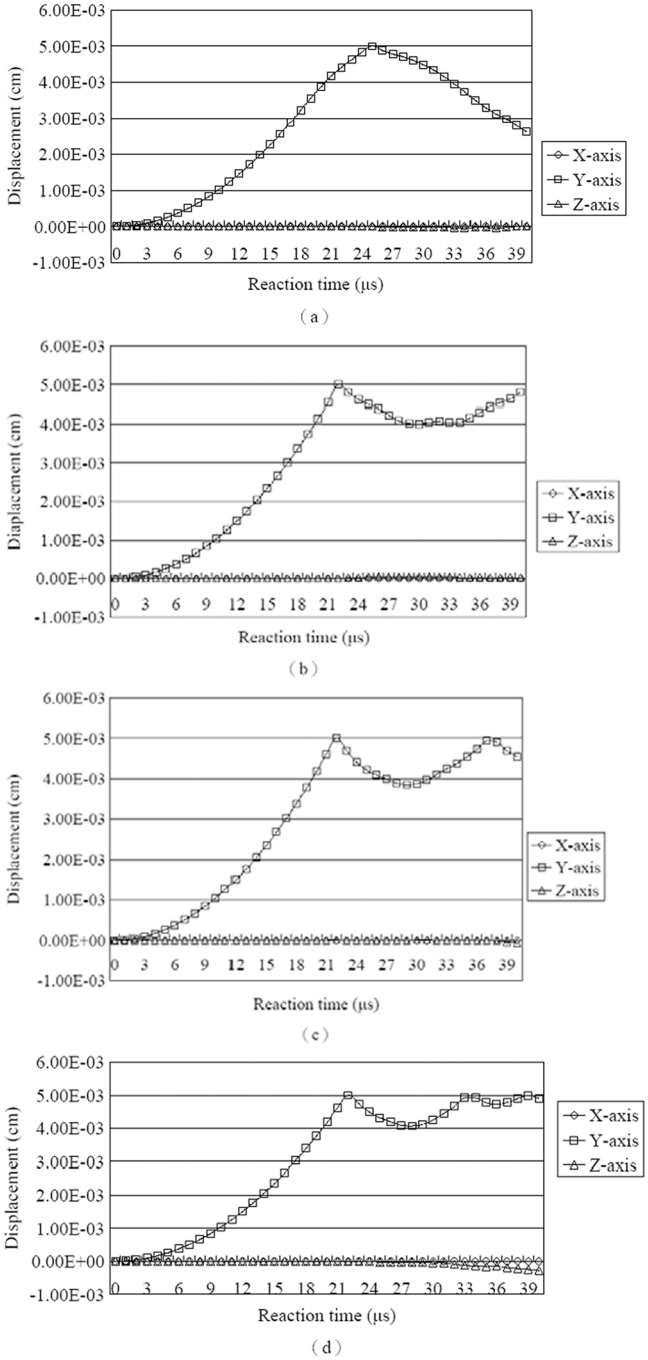

Fig. 8. Displacement of the sensors at 21 000G: (a) type 1; (b) type 2; (c) type 3; and (d) type 4.

deceleration data (shock G value) can be related to the material characteristics of the target using Forrestal's model [9]–[11]

$$a_{\max} = \frac{F}{M} = \frac{\pi d^2 S f_c \left[1 + \left(\frac{I}{N}\right)\right]}{4M} \tag{3}$$

where $a_{\max}$ is the maximum deceleration of the projectile, d is its diameter, M is its mass, N is its geometric function, and S, fc, and I are target-related constants. Table III presents the maximum decelerations of four target materials.

In the simulation, a projectile carrying this smart sensor was arranged to hit targets made of the materials listed in Table III,

TABLE III
DECELERATION DATA FROM FORRESTAL'S MODEL

Target material	d	S	fc	I	N	M	a_{max}
Wood	0.35	38.9	4.00E+06	5.55	189.55	500	3141
Brick	0.35	18.9	1.50E+07	3.04	34.61	500	6065
Concrete	0.35	9.7	5.10E+07	1.74	25.27	500	10412
Aluminum	0.35	3.7	2.95E+08	0.78	29.71	500	22260

Unit： d→m, S→dimensionless quantity, fc→Pa, I→dimensionless quantity, N→dimensionless quantity, M→kg, a_{max} →G value.

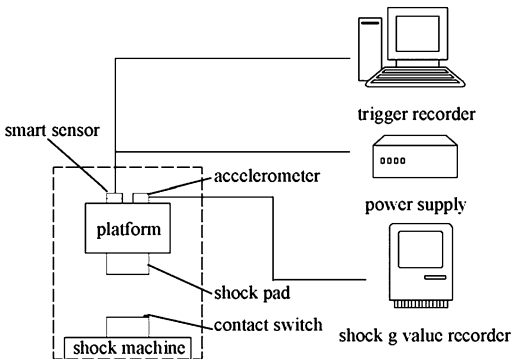

Fig. 9. Shock test system.

with a 0.8 Mach striking velocity. The deceleration data were calculated using formula (3).

V. SHOCK TEST

The smart sensor was placed on the MTS shock test machine (MTS 848), which can be used for performing shock tests at up to 30 000. This shock test machine was used to determine the G value for use in the simulation when the projectile penetrated the target.

The shock test was performed using the system shown in Figs. 9 and 10. The G value is varied by adjusting the height through which the sensor falls or by changing the shock pad. In the original design, when the shock G value is between 3000 and 4000, only the type 4 sensor is triggered and the triggering signal is transmitted to DSP. Similarly, when the shock G value is between 5000 and 7000, type 3 and type 4 sensors are triggered, and the triggering signal is transmitted to DSP. Comparing the signals collected at DSP indicates that the materials in the targets could be identified, as shown in Table IV.

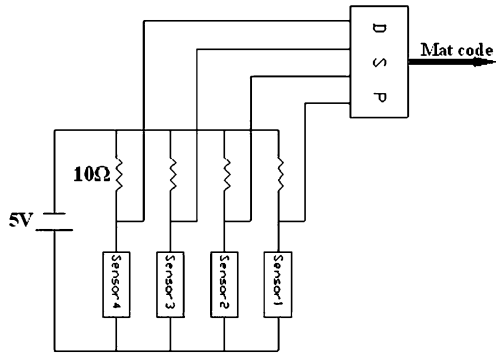

Fig. 10. Test circuit schematic.

TABLE IV
SHOCK TYPE RESULTS

Sensor type	G value				Material Code
	3000~4000	5000~7000	8000~10000	>20000	
Type 4	trigger	trigger	trigger	trigger	00
Type 3	×	trigger	trigger	trigger	01
Type 2	×	×	trigger	trigger	02
Type 1	×	×	×	trigger	03

VI. CONCLUSION

This study presents four G sensors, which are designed to trigger at G = 3000–21 000. Silicon is used as the structural material of the sensor and the triggering mechanism involves a cantilever and a spring structure. The mechanical sensitivity was adjustable and four high G sensors, each operated at a particular G level, are combined with a digital signal processor to construct a smart sensor. The smart sensor identifies materials in hard object when a projectile makes an impact on a hard object.

ACKNOWLEDGMENT

The authors would like to thank Dr. M.-H. Chiu, National Taiwan University, for advice regarding the simulation.

REFERENCES

[1] Y. P. Wang, "Design of a non-powered MEMS high g shock sensor," presented at the ASME 2nd Integration & Commercialization of Micro & Nano Systems Int. Conf. Expo., Kowloon, Hong Kong, Jun. 3–5, 2008.
[2] W. S. N. Trimmer, "Microrobots and micromechanical systems," *Sens. Actuators*, vol. 19, no. 3, pp. 267–287, 1989.
[3] Y. P. Wang, "Design, simulation, fabrication and test of a MEMS-based high G inertial shock sensor," presented at the Int. Conf. Manufacturing and Engineering Systems, Huwei, Taiwan, Dec. 17–19, 2009.
[4] K. S. Min and H. L. Min, "Real-time identification of a medium for a high-speed penetrator," U.S. Patent 5255608, Oct. 26, 1993.
[5] D. R. Ask eland, *The Science and Engineering of Materials*, 1st ed. Taipei, Taiwan: Kai Fa, 1985, ch. 6, pp. 126–127.
[6] M. Elwenspoek and R. Wiegerink, *Mechanical Microsensors*. Berlin, Germany: Springer-Verlag, 2001.
[7] Explicit Dynamics With ANSYS/LS-DYNA Training Manual1st ed. 2001.
[8] T.-R. Hsu, *MEMS & Microsystems Design and Manufacture*. New York: McGraw-Hill, 2002, pp. 157–159.

[9] M. J. Forrestal, B. S. Altman, J. D. Cargile, and S. J. Hanchak, "An empirical equation for penetration depth of ogive-nose projectiles into concrete targets," *Int. J. Impact Eng.*, vol. 15, pp. 395–405, 1994.
[10] D. J. Frew, S. J. Hanchak, M. L. Green, and M. J. Forrestal, "Penetration of concrete targets with ogive-nose steel rods," *Int. J. Impact Eng.*, vol. 21, pp. 489–497, 1998.
[11] M. J. Forrestal, D. J. Frew, J. P. Hickerson, and T. A. Rohwer, "Penetration of concrete targets with deceleration-time measurements," *Int. J. Impact Eng.*, vol. 28, pp. 479–497, 2003.

Y. P. Wang was born in Chiayi, Taiwan, on December 14, 1969. He is pursuing the Ph.D. degree at the Department of Mechanical Engineering, National Chiao Tung University, Hsinchu, Taiwan. The main topic of his study is inertial shock sensor.

R. Q. Hsu is a Professor at the Department of Mechanical Engineering, National Chiao Tung University, Hsinchu, Taiwan.

His research interests include sheet metal forming, and mechanical design of small devices.

C. W. Wu is an Assistant Professor of Mechanical and Mechatronic Engineering at the Department of Mechanical Engineering, National Chiao Tung University, Hsinchu, Taiwan. He is also the Administrator of the common Nano-electro-Mechanical-Systems Laboratory, National Taiwan Ocean University. His research interest is now focused on sensors and actuators, aquatic MEMS, RFID packaging, and nanoimprinting.